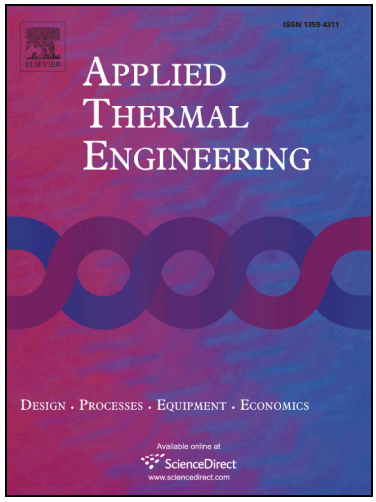

Experimental and Numerical Investigation of a Thermocline Thermal Energy Storage Tank

J.-F. Hoffmann, T. Fasquelle, V. Goetz, X. Py

PII: S1359-4311(16)34046-7
DOI: http://dx.doi.org/10.1016/j.applthermaleng.2016.12.053
Reference: ATE 9673

To appear in: *Applied Thermal Engineering*

Received Date: 13 April 2016
Revised Date: 8 December 2016
Accepted Date: 11 December 2016

Please cite this article as: J.-F. Hoffmann, T. Fasquelle, V. Goetz, X. Py, Experimental and Numerical Investigation of a Thermocline Thermal Energy Storage Tank, *Applied Thermal Engineering* (2016), doi: http://dx.doi.org/10.1016/j.applthermaleng.2016.12.053

Experimental and Numerical Investigation of a Thermocline Thermal Energy Storage Tank

J.-F. Hoffmann [a, b, c]*, T. Fasquelle [a], V. Goetz [a], X. Py [a]

[a] *PROMES-CNRS UPR-8521 Laboratory, University of Perpignan Via Domitia, Rambla de la Thermodynamique, Tecnosud, 66100 Perpignan, France*

[b] *AQYLON, 46-48 rue Renée-Clair, 75892 Paris, France*

[c] *EDF - R&D, MFEE - Nouvelles Filières de Production et Thermochimie, 6 quai Watier, 78401 Chatou, France*

* Corresponding author. Tel: (+ 33) 4 68 30 77 34. E-mail address: thomas.fasquelle@promes.cnrs.fr

Abstract

Thermocline thermal energy storage technology consists in separating hot fluid from cold fluid thanks to a clever use of buoyancy forces. The energy is therefore stored in one tank instead of two and the tank can be filled with solid materials to cut costs. However, the storage efficiency depends on several parameters such as the fluid mass flow and the size of the particles. In the present study, an experimental investigation has been performed in order to know how these parameters influence the size of the thermocline and the efficiency during charging and discharging. Various mass flows, from 0.01 $kg.s^{-1}$ to 0.05 $kg.s^{-1}$ were tested and two different size of particles were investigated (diameters of 12 mm and 40 mm, respectively). As a conclusion, the smaller the particle size, the better the storage efficiency, due to better heat transfer between fluid and solid. An optimum velocity can be found for each configuration of the tank: below this value, heat losses are too important, and above this value thermal flux carried by the forced convection of the heat transfer fluid is too important in comparison with the heat flux exchanged between fluid and solid. A previously validated numerical model has been used in order to verify its capacity of predicting the thermocline behavior, and in order to better understand the influence of the studied parameters on the

storage performances. The model limits were found for high mass flows. It has been also shown that the mass flow needs to be chosen in accordance with the particle diameter in order to have maximum efficiency.

Keywords

Concentrated solar power (CSP), Thermal energy storage (TES), Thermocline, Numerical Modeling

1. Introduction

The main drawback of renewable energies is the variation of their production with time. Efficient, low-cost energy storage technologies must be developed in order to make renewable energies competitive. Concentrated solar power (CSP) seems to be suited to solve this issue, since it produces heat before electricity [1]. Since heat is relatively easy to store, it is theoretically possible for CSP plants to produce electricity with a constant power [2]. In today's most common CSP plants, thermal energy storage consists in two large tanks [3] which can store 7 hours of energy production for a cost that can attain 20% of the whole plant [4,5]. Thermocline thermal energy storage consists in using only one tank instead of two. The hot fluid at the top of the tank is hence separated from the cold fluid at the bottom by a zone with intermediate temperature called thermocline [6]. Filling the tank with solid materials makes it possible to reduce the cost of the thermal energy storage system. It also maintains the thermal stratification in stand-by periods. Solid materials slightly increase the pressure drop; Bruch et al [7] found a maximum of 140 mbars pressure drop, for an oil at 41 °C flowing at 2500 $kg.h^{-1}$, through a 3 meters height and 1 meter diameter thermocline tank. The system efficiency depends on the thickness of the thermocline, which shows the significance of the thermal diffusion. A thorough understanding of the behavior of the thermocline is therefore

needed. Numerical parametric studies have been performed in order to know the key parameters influencing the thermocline behavior. Yang et al [8] studied the effect of the Reynolds number on storage performances and showed there was some optimal Reynolds number for a tank. They also investigated the importance of the heat losses, especially when the fluid flow is very low. Xu et al [9, 10] investigated many parameters in their numerical study. They did not find a significant dependency of the efficiency with the fluid velocity, nor with the inlet temperature. They also investigated the effect of the solid conduction and of the heat transfer between fluid and solid, by comparing different correlations. They also found an optimum porosity at 0.22 and an optimum particle diameter of 19 mm [11]. Flueckiger et al [12] also investigated the particle diameter effect and came to the same conclusion. They also assessed the tank wall condition impact and concluded that heat losses lead to non-negligible entropy generation and lower the thermocline tank efficiency. Despite the numerous numerical results, there is a lack of experimental results to fully understand these phenomena. Among the few experimental tanks built over the past years [6, 13-17], experimental data is scarce. Basically, only two large-scale experiments are considered in the open literature as "references": the thermocline tank from Sandia National Laboratory [6] and the Solar One power plant thermocline tank [13, 14]. Even if limited to very specific working conditions, they provided enough data to compute models and to compare simulations with experimental results.

In this work, an experimental thermocline thermal energy storage tank previously built [18] is working, giving a large set of different experimental conditions in terms of fluid velocity, solid characteristic dimensions and charge or discharge phases. The objectives are: (i) to confirm or deny through the experiments the performances expected with the solid thermocline storage concept; (ii) to compare systematically experimental and simulated thermal behavior of the tank storage in order to validate a simple but robust one dimensional

model based on the thermal balances applied to the liquid and solid phases. Such a model has already been tested with success when applied to Solar One and Sandia National Laboratory thermocline storage tanks [18].

2. Model description

The present numerical study is based on the model developed in our previous paper [18]. The numerical model treats two distinct systems inside the tank: the fluid 'f', the solid 's' and one additional system formed by the wall 'w'. The fluid flow inside the tank is considered uniform and one directional. Continuity and momentum equations are not resolved, but the local oil speed is calculated from the mass flow and the local density. The solid filler is considered as a continuous, homogenous and isotropic porous medium [9, 19]. Radial heat losses and thermal inertia of the tank are taken into account with a balance applied to the wall of the storage. It has been shown in a previous study [18] that these assumptions do not prevent the model from predicting the thermocline thermal behavior.

3. The built experimental tank

The laboratory-scale experiment built at the PROMES-CNRS laboratory is depicted in Fig. 1, and all its main characteristics are summarized in Table 1 [18]. The tank was filled with quartzite rocks, with a porosity of around 0.4. Rapeseed oil and quartzite rock characteristics are summarized in Table 2 [14, 20]. The void fraction was occupied by rapeseed oil. The tank wall mass is approximately 150 kg, including flanges, and was insulated with 20 cm of rock wool covered with aluminum foil. The temperature inside the tank is measured using 32 thermocouples. Radial temperature variations were negligible, less than 3 °C temperature drop between the center and the temperature of the thermocouple near the external surface. Temperature data was therefore collected at the axial center from 2 cm above the bottom of the filler to the top of it. The step between two thermocouples was 16 cm

and their uncertainty was 1 °C. Heaters of 9 kW total thermal power heat the oil before sending it to the tank and an air heat exchanger with 25 kW capacity can cool down the oil exiting the tank during a discharge process. The flow was measured with a Brooks MT 3809 flow meter calibrated with respect to the temperature of the fluid flowing through, to an accuracy of ± 10%.

Figure 1

Table 1

Table 2

4. Experimental investigations

4.1 The parametric study

Two particle sizes have been investigated. The tank was first filled with 325 kg of quartzite rocks with an average diameter G40 of 0.04 m. The ratio between the tank diameter and the particle diameter was therefore 10. Then it was entirely emptied, rapeseed oil was also replaced by another one, and the tank was filled again with 340 kg of quartzite rocks with an average diameter G12 of 0.012 m. The ratio between the tank diameter and the particle diameter was therefore 33.3. The porosities were calculated from the solid material masses and from the filler bed volume; they were equal to 0.41 and 0.39 for the G40 and G12 particles, respectively. If as expected, porosity was almost independent of the particle size in the case of a uniform arrangement, particle diameter is a key parameter in a dual-media thermocline. The smaller the particles, the larger the heat transfer surface i.e.: 20 m² for G40 and 68 m² for G12 considering the total surface exchange between the solid and the fluid in the tank.

The inlet fluid velocity is another key parameter for this type of thermal energy storage, since this operating condition is likely to change a lot in a real power plant. Basically, the thermal energy storage must tolerate a wide range of velocities without an efficiency decrease to be suited to concentrated solar power plants. In this study, we therefore investigated the thermocline behavior with the fluid velocity. To do so, five inlet velocities, controlled using a pump and feedback from the flowmeter, were experimentally studied, for the two particle sizes. Regarding the Biot number, with values ranging between 0.054 and 0.031 whatever the fluid velocities and particle sizes, no heat transfer limitation has to be taken into consideration [19].

4.2 The outlet parameters

For each case studied, the five different inlet velocities applied to the particles of two different sizes, the thermocline evolution with time, the outlet temperature and the thermal energy storage efficiency have been depicted and compared to numerical results. Basically, discharge efficiency can be defined in different ways in a thermocline case. Since the outlet temperature decreases during the discharge process, a threshold beyond which the energy is deemed not useful had to be chosen. This high threshold depends on the element that is upstream the thermocline tank (for example a power block in a thermal power plant) and which defines the working conditions of the storage. Equation 10 defines the chosen threshold of the present study (as in [10]).

$$T_{high\_threshold} = T_L + 0.8 \cdot (T_H - T_L) \ , \tag{10}$$

The efficiency is then defined by the following equation:

$$\eta_{discharge} = \frac{E_{discharged}\left[T_{outlet} > T_{high\_threshold}\right]}{E_{initially\_charged}} \ . \tag{11}$$

$E_{discharged}$ is the energy delivered during the discharging process while respecting the high threshold value. The initially charged energy $E_{initially\_charged}$ is calculated from the initial temperature profile in the tank. With this definition, the discharge efficiency corresponds to the useful energy in the tank. The remaining energy is not lost but cannot be used in the downstream process without increasing the fluid temperature. Because of propagation of uncertainty, the discharge efficiency uncertainty is about 15%.

For the charging process case, another threshold temperature can be defined and corresponds to the maximum allowed inlet temperature of the solar field. Above this low temperature threshold in the inlet of the solar field, there is a risk of overheating the heat transfer fluid during its travel in the receivers. In the present study, we chose to define this threshold as follows:

$$T_{low\_threshold} = T_L + 0.2 \cdot (T_H - T_L), \quad (12)$$

Charging efficiency is then defined by the following equation.

$$\eta_{charge} = \frac{E_{finally\_charged}\left[T_{outlet} < T_{low\_threshold}\right]}{E_{max}}. \quad (13)$$

The finally charged energy $E_{finally\_charged}$ is the energy stored during the charging process while respecting the low threshold value. E_{max} corresponds to the maximum energy the tank could store if it was fully at the high temperature. It should be noted that a tank entirely at low temperature is considered as filled with no energy. The charge efficiency uncertainty is also about 15%.

The thermocline size is also a characteristic of interest. Thermocline size is defined as the part of the tank in which the temperature is between the two thresholds.

$$H_{tc} = \begin{Bmatrix} H_{T_{90\%}} - H_{T_{10\%}}; T_{in} \leq T_{10\%} \;\&\; T_{out} \geq T_{90\%} \\ H_{T_{90\%}} - 0\,; T_{in} > T_{10\%} \\ H - H_{T_{10\%}}; T_{out} < T_{90\%} \end{Bmatrix}. \quad (14)$$

This parameter is highly relevant because it reflects the energy storage efficiency. The thinner the thermocline size, the bigger the two isothermal zones and the greater the efficiency. The thermocline height is therefore a parameter to minimize. Because of the 16 cm step between two thermocouples, the thermocline thickness uncertainty is about 32 cm. However, we decided to use a linear interpolation to better locate the threshold heights between two thermocouples.

With all these definitions, it is possible to understand and compare the different behaviors of the thermal energy storage tank, for the discharge and for the charge.

5. Results

5.1. Thermocline behavior in a discharge

The different temperature profiles for a discharge of the tank filled with small particles (G12) and a low mass flow ($1.9.10^{-2}$ kg.s^{-1}) are depicted in Fig. 2, against the tank height. One curve is drawn every half hour, from left to right. Numerical results are compared to experimental ones in order to check the validity of the model.

Figure 2

Results showed all the different steps of a thermocline discharge. At the initial time, the tank was almost entirely at high temperature. One hour later, thermocline had been created, with a constant low temperature at the bottom of the tank and a nearly constant high temperature at the top of the tank. The thermocline therefore corresponded to the intermediate region, with a very important temperature variation. The hot region was not totally constant

because of heat losses, which were very important in comparison to the tank size. This would be less visible with bigger tanks but corresponds to a reality that must not be neglected. It can then be seen from the following curves that the thermocline region was moving through the tank, and thermal diffusion was occurring, which implied a decrease of the slope of the thermocline region. Finally, about two hours after starting the discharge, the hot region had been extracted, the thermocline region started to leave the tank, and the outlet temperature started to decrease very quickly.

5.2. Influence of the mass flow

With another mass flow ($5.3\ 10^{-2}$ kg.s^{-1}) we obtained the temperature profiles depicted on Fig. 3. In order to compare the discharge rates, the same time steps between two temperature profiles (0.5 hour) have been chosen. The discharge time is obviously lower for the high mass flow experiment, but the thermocline slope seems to be roughly the same.

Figure 3

The outlet fluid temperature and the output power for the two experiments are depicted against time in Fig 4. The two depicted outlet temperatures first endured slow decreases, and then dropped when the thermoclines were extracted. The high mass flow experiment obviously showed a faster discharge. The output power for the high mass flow started at a higher value then underwent a very fast decrease, due to the decreasing outlet temperature. The outlet power for the low mass flow started at a lower value but stayed almost constant for almost 2.5 hours, then also decreased when the thermocline reached the outlet. For the low mass flow experiment, during the two first hours, the decreasing output power and temperature were mainly due to heat losses. The numerical results showed a relatively good accordance with the experiment results, with a maximum discordance of 5.3 °C for the highest mass flow. For that high mass flow, the model predicted better heat

transfer between fluid and solid and it resulted in higher power and outlet temperatures at the beginning and lower ones at the end of the discharge.

Figure 4

For a cut-off temperature of 200 °C, the first experiment *(a)* showed a discharge efficiency of 69% when the second *(b)* was 72%. It can be explained by the thermocline region heights, which were not the same for the two experiments and were depicted against time in Fig. 5.

Figure 5

In Fig. 5, it can be seen that a discharge can be broken down into two parts: thermocline expansion while shifting and thermocline exit. The initial thermocline thicknesses were not equal to zero because of the non-uniform temperatures inside the tank (it was impossible to attain uniform temperatures in practice) at the beginning of the discharge phase. Depending on the fluid mass flow, these parts did not have the same duration, and the maximum thermocline thickness was not the same, with a height of 1.3 m for the low mass flow experiment and 0.8 m for the high mass flow experiment. Since the higher the thermocline thickness, the lower the discharge efficiency, it can be concluded from this graph that the higher mass flow rate implied a better efficiency. Fluid mass flow did have an influence on the thermocline discharge efficiency. Discharge efficiency for the G12 granulometry and with five different inlet velocities was depicted in Fig 6. Experimental efficiencies were compared to simulated ones. Moreover, simulations carried out in the case of a perfectly insulated tank were added.

Figure 6

There was an optimum mass flow for maximum efficiency. With a lower mass flow, the efficiency decreased significantly. This decrease was mainly due to heat losses, but also to the growing influence of the diffusion with the decrease of the mass flow. With higher mass flows, the heat transfer exchange between fluid and solid particles is too low in comparison to the heat fluxes transported by forced convection of the fluid. Simulations performed for adiabatic walls clearly brought to light these last two phenomena and their respective influence. Numerical model with heat losses did a reasonable prediction of the thermocline efficiency for discharges in the whole range of tested mass flows. The mass flow optimum value is not reached because of the overestimated heat transfers between fluid and solid for the high mass flow experiments. Nevertheless it can be considered that the thermocline thermal energy storage can operate at quite good efficiency with a varying inlet fluid mass flow. These results confirmed the assumptions made by Yang et al [8], who performed numerical parametric studies of thermocline tanks.

5.3. Influence of the granulometry

The different temperature profiles for a discharge of the tank filled with bigger particles, with an average diameter of 40 mm (G40) and with a mass flow of 4.9 $kg.s^{-1}$ were depicted in Fig. 7.

Figure 7

The thermocline size increase was more visible than in Fig. 3 because of the smaller exchange surface between the fluid and the solid. For this experiment, the outlet temperature and the discharge efficiency were depicted in Fig 8. The inlet temperature was added to the figure because it was not totally constant during the experiment. This kind of representation previously depicted in the case of another application of thermocline [21] shows the discharge efficiency for a chosen temperature threshold. For a discharge threshold of 20%,

corresponding to a threshold outlet temperature of 200 °C, the discharge efficiency was 67%, against 72% for the G12 granulometry. For a higher cut-off temperature of 205 °C, the discharge efficiency was 58%. Obviously, the discharge efficiency depends heavily on the cut-off temperature.

Figure 8

Thermocline sizes over time for the two granulometries and for one mass flow (4.9 – 5.3 $kg.s^{-1}$) are depicted in Fig. 9. Basically, for the G40 granulometry, changes of the thermocline thickness followed three distinct steps: formation, shifting and exit. When the tank was totally charged at T_H, the inlet heat transfer fluid at low temperature T_L created the thermocline. The heat front formation, formally the length necessary to the increase of the fluid temperature to the desired threshold entailed an important increase of the thermocline thickness. It occurred from the beginning of the discharge to around 0.2 hours. When the thermocline was created, it moved along the axial direction over the time. During this shifting, thermal diffusion resulted in a gradual increase of the thermocline thickness. After 0.7 hours of discharge, the thermocline zone exited the tank and therefore its thickness decreased until total extraction of the thermocline. For the G40 configuration, thermocline size reached its maximum of 1.09 m, or 60% of the rock bed height, after 1.2 hours of discharge. For the G12 configuration, thermocline size reached 0.82 m, or 46% of the tank height, after 1.3 hours of discharge. A better heat transfer therefore induces a better separation of the two isothermal zones in the tank, and so a higher efficiency.

Figure 9

From the experiments, it can be seen that the maximum discharge efficiency that can be obtained with the G40 granulometry was lower than in the case of G12 granulometry. This

confirmed the fact that a higher area of heat exchange implies higher efficiencies. Figure 10 shows the discharge efficiency against mass flows for the G40 granulometry.

Figure 10

As for the G12 granulometry, there was an optimal mass flow at which the discharge efficiency was the highest. This optimal mass flow for the G40 granulometry was not the same as for the G12 granulometry, because since the particles are bigger for the G40 granulometry, heat transfer between fluid and solid was lower, and the ratio between the flux transported by the fluid and the flux exchanged between fluid and solid was higher. The numerical results enabled to give a tendency of the efficiency curve, with a maximum discordance of 10%, which is within the calculated experimental efficiency uncertainty.

5.4 Charging process results

Two charging processes are presented in Fig 11. The two experiments had the same conditions apart from the particle diameters. The initial temperature profiles are also different. Temperature profiles have to be read from right to left. From a cold tank to a hot tank, thermocline creation, expansion and exit can again be observed.

Figure 11

The numerical results were very close to the experimental ones. The heat losses were less visible for the charging process than for the discharging process, since the charging process starts with a low temperature tank. It was therefore easier to simulate charging behavior than discharging behavior. An adiabatic model would have also agreed acceptably with the experimental results for the charging mode. A cut-off temperature corresponding to a 20% increase of the total temperature difference has been chosen in this study. A higher outlet temperature is considered unacceptable for the downstream element (risk of overheating the

heat transfer fluid for example). It was thus not possible to totally fill the tank with high temperature heat transfer fluid and a part of the tank was not used. Fig. 12 shows the charging efficiency, the outlet temperature and the inlet temperature for two charging experiments. After including the varying inlet temperatures into the model, there was significant accordance between the numerical results and the experimental ones. The charging efficiency for a cut-off temperature of 170 °C was 74% for G12 against 72% for G40 granulometry. It means that, in every case, more than one quarter of the tank was not used to store energy at a sufficient temperature level.

Figure 12

5.5. Model investigation

Since the thermal model showed its robustness and since experimental investigation showed that there is an optimal mass flow that enables a maximum efficiency for each particle size, we decided to perform a numerical study on this optimal mass flow. For each particle size from 1 cm to 10 cm, with a 1 cm step, the mass flow was varied from 0.01 $kg.s^{-1}$ to 0.1 $kg.s^{-1}$ with a 0.01 $kg.s^{-1}$ step, and the highest efficiency case was searched. Previous simulations were carried out in order to compare their results to the experimental ones and therefore started with a particular temperature profile. In this case, each simulation started with a full load tank at 210 °C, by sending cold oil at 160 °C. Figure 13 depicts this optimal mass flow and the corresponding discharge efficiency, for each tested particle size.

Figure 13

It can be seen that of course the smaller the particle the higher the efficiency, without taking into account the pressure losses. When increasing the particle size, the mass flow has to be decreased in order to give time to the heat exchange to process. This kind of figure may

enable to define a working point for a specific tank, but can hardly be extended to other tanks, with different size, working fluid and solid medium.

6. Conclusion

This study has carried out an experimental investigation of the behavior of a thermocline thermal energy storage tank. To do so, a laboratory scale tank was built. It has a thermal capacity of 8.3 kWth and can perform from 1 to 5 hours of charging and discharging processes. Filled with quartzite and rapeseed oil as heat transfer fluid, the experimental tank was working in a temperature range of 160 °C – 210 °C. This demonstrator made it possible to perform a parametric study regarding the size of the particles and the inlet fluid velocity.

At first, thermocline behavior during a discharge was explained using experimental temperature profiles. Thermocline formation, expansion while shifting and exit were described and the influence of heat losses was observed.

Influence of the fluid mass flow was assessed using different experimental results for one granulometry. It has been confirmed that thermocline tanks present an optimum mass flow corresponding to maximum discharge efficiency. In the present case, the maximum discharging efficiency for the G40 granulometry was found to be 75%, with a mass flow of 0.3 $kg.s^{-1}$. Lower mass flows imply higher significance of heat losses and thermal diffusion. Higher mass flows imply a discrepancy between the heat fluxes transported by forced convection of the fluid and the heat transfers between the fluid and the solid particles. Comparing two experimental discharges with different particle sizes and with the same mass flow also made it possible to assess the influence of the granulometry. For a given cut-off temperature, the discharge efficiency for the small granulometry was higher, thanks to

naturally larger exchange surface between fluid and solid and therefore a better heat transfer rate between them. The maximum thermocline thickness was therefore lower. Different optimum mass flows were found for both granulometries, and the higher efficiency was again found for the small particle experiment.

Similar experiments were performed for the charging process. A charging efficiency of 74% was found for the G12 granulometry, while a value of 72% was found for the G40 granulometry.

In every case, experimental results were compared to numerical ones from a previously developed model, with no parameter fitting process. Results were in good accordance, despite some small limitation of the numerical model with high mass flows.

Finally, a numerical study was performed in order to provide a tool that can give the optimal mass flow with maximum discharge efficiency. It showed that the bigger the particle, the lower the optimal mass flow.

Acknowledgments

The project was supported financially by ANRT (ANRT CIFRE n°2012/1516) for a PhD grant through a CIFRE program, AQYLON and EDF R&D. This work was also supported by the Program “Investissements d’avenir” (Investment for the Future) of the Agence Nationale de la Recherche (National Agency for Research) of the French State under award number ANR-10-LABX-22-01-SOLSTICE.

The authors would like to thank A. Bouvier d’Acher for the demonstrator experimentation and. G. Hernandez, J.-J. Huc, and J.-M. Mancaux for their help in building the demonstrator.

Notation

Dimensionless numbers

Bi	Biot number [-]
Pr	Prandtl number [-]
Re	Reynolds number [-]

Greek letters

μ	Dynamic viscosity [Pa s]
ρ	Density [kg m^{-3}]
ε	Void fraction [-]
η	Efficiency [-]

Latin letters

$\dot{m}$	Mass flow rate [kg s^{-1}]
A	Area [m^2]
C_p	Specific heat [J kg^{-1} K^{-1}]
D	Diameter of packed bed [m]
d_p	Diameter of particles [m]
E	Energy [J]
H	Height of packed bed [m]
h_{ext}	Coefficient of thermal losses to the environment [W m^{-2} K^{-1}]
Htc	Thermocline height [m]
h_v	Interstitial heat transfer coefficient [W m^{-3} K^{-1}]
h_w	Heat transfer coefficient through the wall [W m^{-2} K^{-1}]
k	Thermal conductivity [W m^{-1} K^{-1}]
R_{th}	Thermal resistance [K W^{-1}]
T	Temperature [°C]
t	Time [s]
u	Velocity [m s^{-1}]
V	Volume [m^3]
x	Axial coordinate of bed [m]

Subscripts

tot	Relative to the whole tank (fluid, solid and wall)
s↔w	Between the solid and the wall
f↔w	Between the fluid and the wall
w↔ext	Between the wall and the outside
air	Air
amb	Ambient
charge	Charge
discharge	Discharge
exp	Experimentation
f	Fluid
H	High
i	Inlet
L	Low
max	Maximum
outlet	Outlet
s	Solid
w	Wall

References

[1] D. Barlev, R. Vidu, and P. Stroeve, "Innovation in concentrated solar power," *Sol. Energy Mater. Sol. Cells*, **95**, 2703–2725 (2011).

[2] M. Medrano, A. Gil, I. Martorell, X. Potau, and L. F. Cabeza, "State of the art on high-temperature thermal energy storage for power generation. Part 2 – Case studies," *Renewable and Sustainable Energy Reviews*, **14**, 56–72 (2010).

[3] S. Kuravi, J. Trahan, D. Y. Goswami, M. M. Rahman, and E. K. Stefanakos, "Thermal energy storage technologies and systems for concentrating solar power plants," *Progress in Energy and Combustion Science*, **39**, 285–319 (2013).

[4] U. Herrmann, B. Kelly, and H. Price, "Two-tank molten salt storage for parabolic trough solar power plants," *Energy*, **29,** 883–893 (2004).

[5] G. Angelini, A. Lucchini, and G. Manzolini, "Comparison of thermocline molten salt storage performances to commercial two-tank configuration," *Energy Procedia*, **49**, 694–704 (2013).

[6] J. E. Pacheco, S. K. Showalter, and W. J. Kolb, "Development of a molten-Salt thermocline thermal storage system for parabolic trough plants," *Journal of Solar Energy Engeering*, **124**, 153–159 (2002).

[7] A. Bruch, J. F. Fourmigué, and R. Couturier, "Experimental and numerical investigation of a pilot-scale thermal oil packed bed thermal storage system for CSP power plant," Solar Energy, 105, 116–125 (2014).

[8] Z. Yang, and S. V. Garimella, "Molten-salt thermal energy storage in thermoclines under different environmental boundary conditions," *Applied Energy*, **87**, 3322–3329 (2010).

[9] C. Xu, Z. Wang, Y. He, X. Li, and F. Bai, "Sensitivity analysis of the numerical study on the thermal performance of a packed-bed molten salt thermocline thermal storage system," *Applied Energy*, **92**, 65–75 (2012).

[10] C. Xu, Z. Wang, Y. He, X. Li, and F. Bai, "Parametric study and standby behavior of a packed-bed molten salt thermocline thermal storage system," *Renewable Energy*, **48**, 1–9 (2012).

[11] C. Xu, X. Li, Z. Wang, Y. He, and F. Bai, "Effects of solid particle properties on the thermal performance of a packed-bed molten-salt thermocline thermal storage system," *Applied Thermal Engineering*, **57**, 69–80 (2013).

[12] S. M. Flueckiger and S. V. Garimella, "Second-law analysis of molten-salt thermal energy storage in thermoclines," *Solar Energy*, **86**, 1621–1631 (2012).

[13] S. E. Faas, L. R. Thorne, E. A. Fuchs, and N. D. Gilbertsen, "10 MWe Solar Thermal Central Receiver Pilot Plant : Thermal Storage Subsystem Evaluation - Final Report," *SAND86-8212*, (1986).

[14] S. Flueckiger, Z. Yang, and S. V. Garimella, "Thermocline energy storage in the solar One power plant: an experimentally valited thermomechanical investigation," Proceedings of the ASME 2011, 1–7 (2011).

[15] A. Meier, C. Winkler, and D. Wuillemin, "Experiment for modeling high temperature rock bed storage," Solar Energy Materials, 24, 255–264 (1991).

[16] M. M. Valmiki, W. Karaki, P. Li, J. Van Lew, C. Chan, and J. Stephens, " Experimental investigation of thermal storage processes in a thermocline tank," Journal of Solar Energy Engineering, 134, 041003–041009 (2012).

[17] G. Zanganeh, A. Pedretti, S. Zavattoni, M. Barbato, and A. Steinfeld, "Packed-bed thermal storage for concentrated solar power - Pilot-scale demonstration and industrial-scale design," Solar Energy, 86, 3084–3098 (2012).

[18] J.-F. Hoffmann, T. Fasquelle, V. Goetz, and X. Py, "A thermocline thermal energy storage system with filler materials for concentrated solar power plants: Experimental data and numerical model sensitivity to different experimental tank scales," *Applied Thermal Engineering*, **100**, 753–761 (2016).

[19] S. Flueckiger, B. Iverson, S. V. Garimella, and J. E. Pacheco, "System-level simulation of a solar power tower plant with thermocline thermal energy storage," *Applied Energy*, **113**, 86–96 (2014).

[20] J.-F. Hoffmann, J.-F. Henry, G. Vaitilingom, R. Olives, M. Chirtoc, D. Caron, and X. Py, "Temperature dependence of thermal conductivity of vegetable oils for use in concentrated solar power plants, measured by 3omega hot wire method," *International Journal of Thermal Sciences*, **107**, 105–110 (2016).

[21] A. Kéré, V. Goetz, X. Py, R. Olives, and N. Sadiki, "Modeling and integration of a heat storage tank in a compressed air electricity storage process", *Energy Conversion and Management*,**13**, 499–510 (2015).

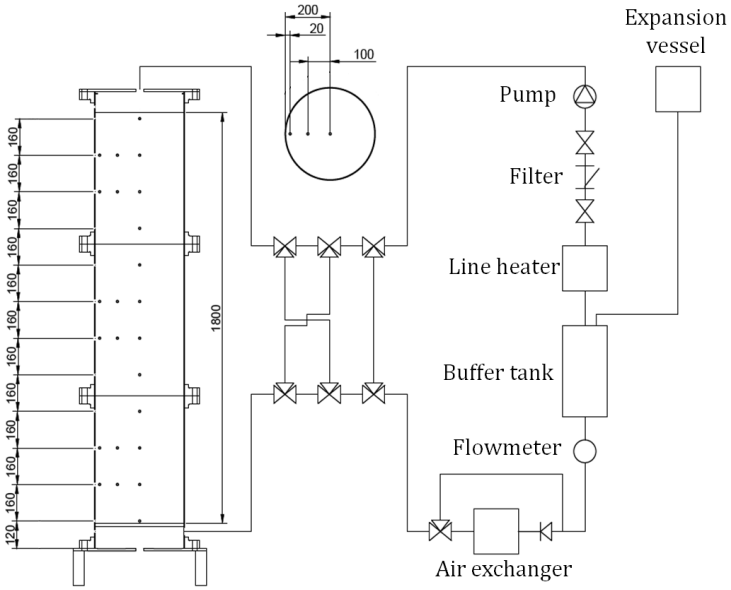

Figure 1: *The present study demonstrator illustrated with the temperature measurement positions and each mechanism.*

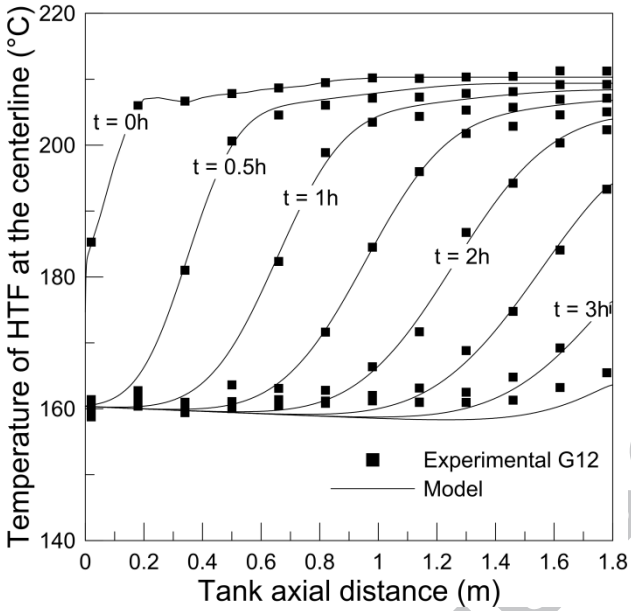

Figure 2: *Temperature profiles at the centerline of the HTF – G12, 1.9 10^{-2} kg.s^{-1}.*

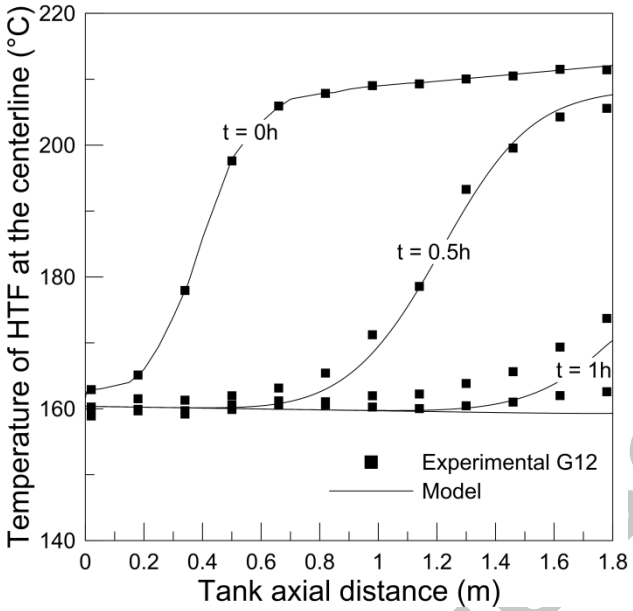

Figure 3: *Temperature profiles at the centerline of the HTF – G12, 5.3 10^{-2} kg.s^{-1}.*

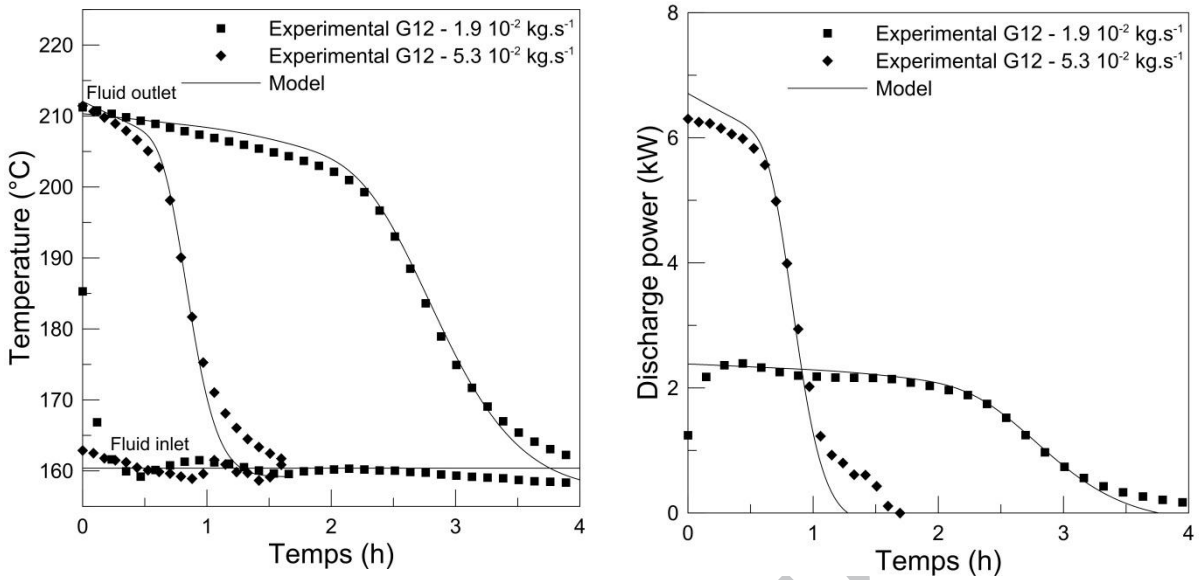

(a) *(b)*

Figure 4: *(a) Inlet and outlet temperature during the discharge, (b) Discharge power G12, 1.9 10^{-2} kg.s^{-1} and G12, 5.3 10^{-2} kg.s^{-1}*

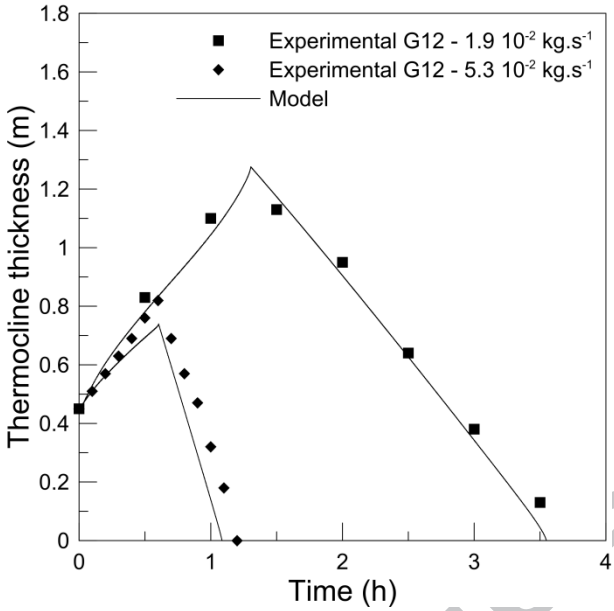

Figure 5: *Thermocline thickness for two fluid mass flow – 1.9 10^{-2} kg.s^{-1} and 5.3 10^{-2} kg.s^{-1}.*

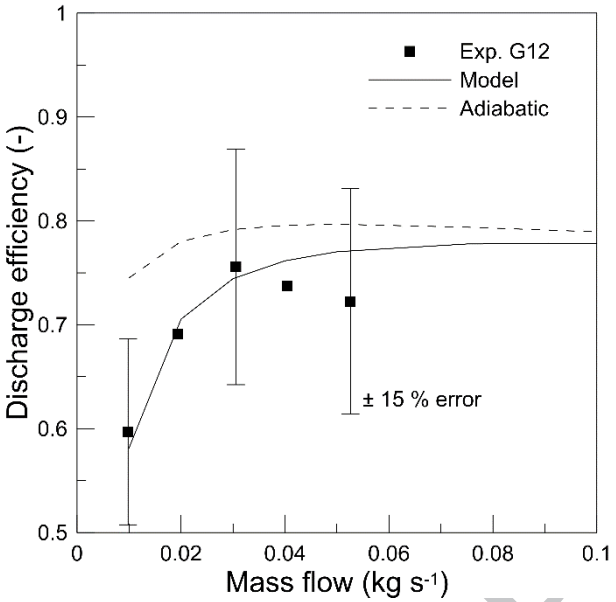

Figure 6: *Discharge efficiency as function of the mass flow for the granulometry G12.*

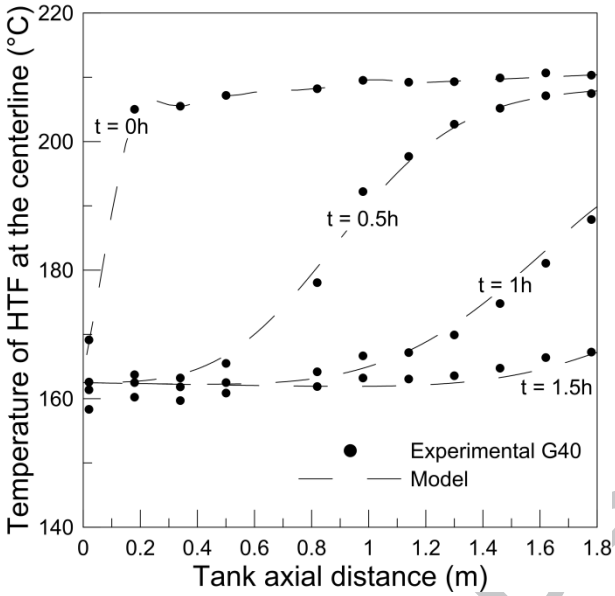

Figure 7: *Temperature profiles at the centerline of the HTF – G40, 4.9 10^{-2} kg.s^{-1}.*

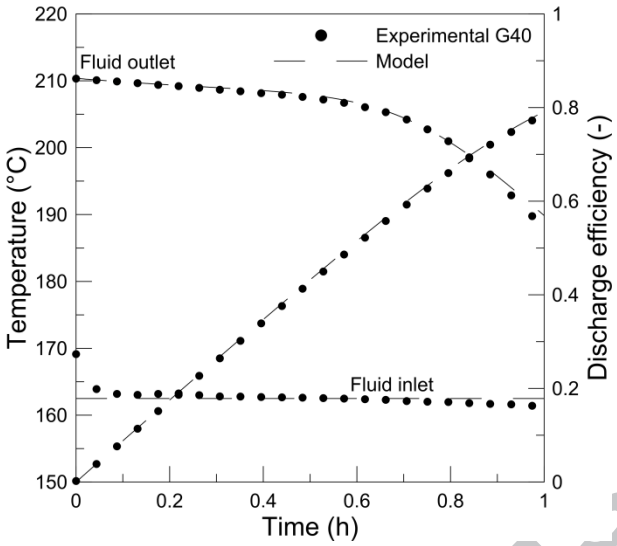

Figure 8: *Inlet, outlet temperatures and efficiency during the discharge – G40, 4.9 10^{-2} kg.s^{-1}.*

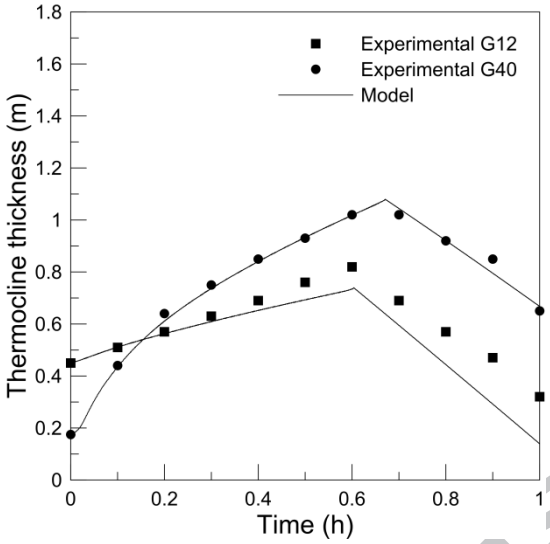

Figure 9: *Thermocline thickness for two discharges (G12, 5.3 10^{-2} kg.s^{-1} – G40, 4.9 10^{-2} kg.s^{-1}).*

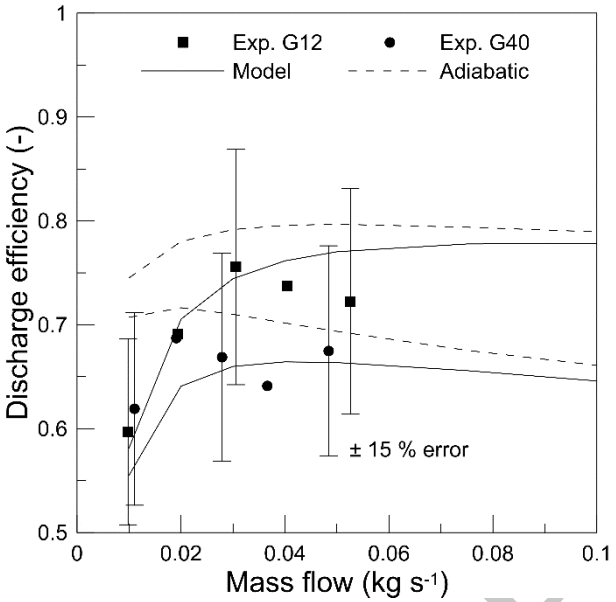

Figure 10: *Discharge efficiency as function of the mass flow.*

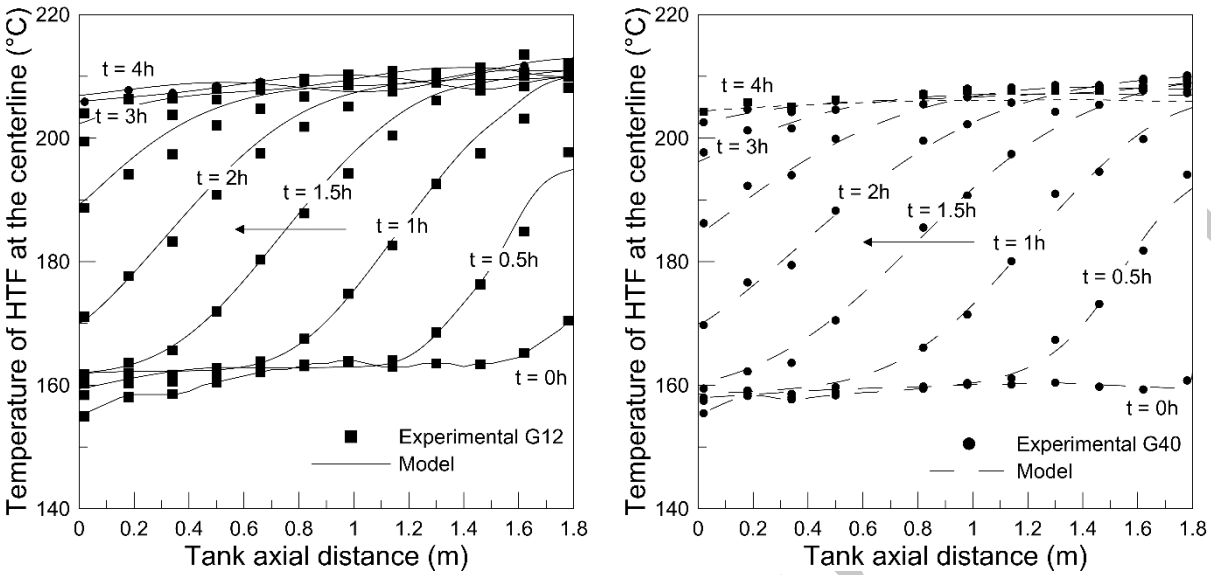

(a) *(b)*

Figure 11: Charging: *Temperature profiles at the centerline of the HTF*

(a) G12, 3.0 10^{-2}kg.s^{-1} (b) G40, 2.9 10^{-2} kg.s^{-1}

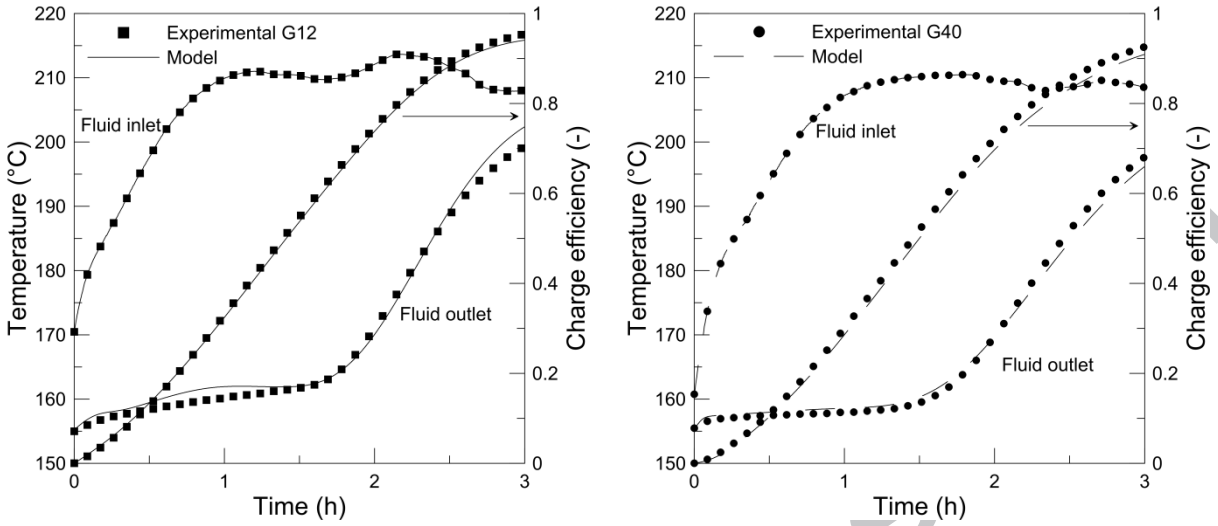

(a) *(b)*

Figure 12: *Inlet, outlet temperatures and efficiency during the charge*

(a) G12, 3.0 10^{-2}kg.s^{-1} (b) G40, 2.9 10^{-2} kg.s^{-1}

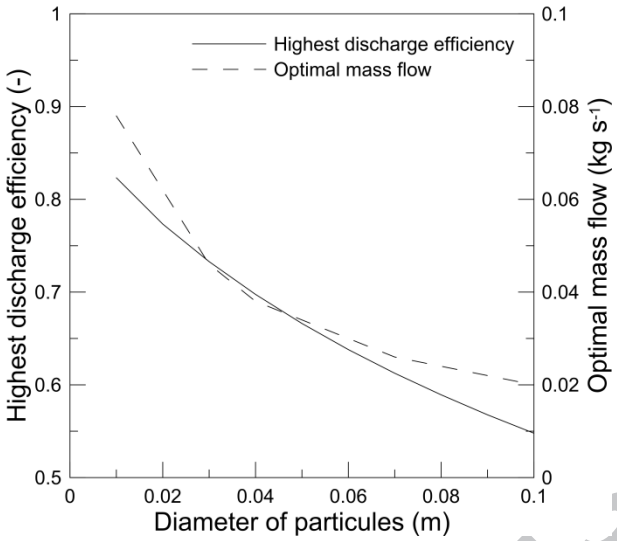

Figure 13: *Highest discharge efficiency and optimal mass flow for any diameter of particles.*

PARAMETER	***PROMES-CNRS Laboratory demonstrator***
Energy	8.3 kWh_T
HTF	Rapeseed oil
TESM	Quartzite rock
Tank height, H	1.8 m
Tank diameter, D	0.4 m
Volume, V	0.25 m^3
Particle diameter, d_p	12 10^{-3} m ; 40 10^{-3} m
HTF mass flow rate, $\dot{m}$	1 10^{-2}– 5.3 10^{-2} kg s^{-1}
TH	210°C
TL	160°C

Table 1: *Main characteristics for the present study demonstrator.*

Rapeseed oil [20]	ρ_f	kg m^{-3}	928.19 - 0.6691 T
	Cp_f	J kg^{-1} K^{-1}	$(1.621 \times 10^{-9} T^4 - 8.735 \times 10^{-7} T^3 + 14.933 \times 10^{-5} T^2 - 5.976 \times 10^{-3} T + 2.0985) \times 1000$
	k_f	W m^{-1} K^{-1}	$2.004 \times 10^{-7} T^2 + 1.713 \times 10^{-4} T + 0{,}1698$
	μ_f	Pa s	$(39\,498\ T^{-1.764}) / 1000$
Quartzite [14]	ρ_s	kg m^{-3}	2500
	Cp_s	J kg^{-1} K^{-1}	830
	k_s	W m^{-1} K^{-1}	5.69

Table 2: *Thermal and thermo-physical properties of the HTF and TESM.*

Highlights

- An experimental and numerical study is performed on a small thermocline tank
- Two particle diameters and five mass flows were tested
- An optimum mass flow/a maximum efficiency is found for the two particle sizes
- The model is used to define the best mass flow for any particle diameter